MVA2007 IAPR Conference on Machine Vision Applications, May 16-18, 2007, Tokyo, JAPAN

A Physics-Based Imaging Model of Scanning Electron Microscopes

Kousuke KAMADA, Takayuki OKATANI, and Koichiro DEGUCHI
Graduate School of Information Sciences, Tohoku University
Aoba-campus, Sendai 980-8579 JAPAN

Abstract

This paper discusses a physics-based imaging model of scanning electron microscopes (SEM). The purpose is to accurately examine the imaging process of a SEM, which has to be necessary to realize novel applications of the SEM images, such as 3D shape reconstruction from image brightness. Its brightness is determined by the total energy of the secondary electrons derived by the incidence of accelerated electron beam to a surface point and then captured by the SEM detector. There are several simple imaging models. But, they are pointed out that the actual brightness cannot be dealt with. We then develop a better imaging model that precisely describes the physical process of the emergence of the secondary electron, their reflections and detections.

1 Introduction

Scanning Electron Microscope (SEM) is a microscope which enables to observe an object of nano-meter size. It projects scanning electron beam onto the object surface placed in vacuum atmosphere. Then, the total energy of the secondary electrons emerging for the incidence of an accelerated electron beam is captured by the SEM detector, and the brightness proportional to the energy is displayed synchronizing with the electron beam scanning. This process is schematically shown in Fig. 1. Example images are also shown in Fig. 2.

There are several imaging models for the SEM images. The most basic one is such that the brightness is represented by the secant of the incident angle of the electron beam to the object surface. This model leads to the possibility of the 3D surface shape reconstruction of the object surface from SEM images. Some reconstruction algorithms have been proposed in the literatures [1, 2, 3, 4].

On the other hand, there are some discussions pointing out that those basic models are too simple because the amount of emerging electron depends also on the detail shape of the surface, and the spatial arrangement of the detector [5, 6].

As shown later in Fig. 13 obtained in our experiments, there exists a case where the planar surfaces having same secant angle generate different brightnesses. For those cases, we need more complicated imaging models. However, almost no discussion has been done from the view point of 3D reconstruction. For the reconstruction, we need proper model which is not too complicated and represents consistent 3D characteristics of the object surfaces.

In this paper, we build up a more reliable imaging model by tracing the physical process from the incidence of the electron beam onto the object surface to the capturing the electrons more detail and accurately. We also show its feasibility by the experiments using simple shape test pieces whose dimensions were known.

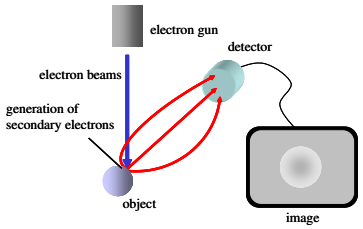

Figure 1: The imaging process of SEM images.

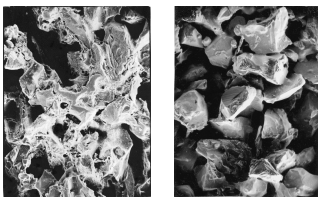

Figure 2: Examples of SEM images.

2 Conventional basic imaging modes

We, first, briefly review some conventional basic imaging models. As the electron beam runs into an object surface, the secondary electrons are emerged from the surface. Because the energy of the secondary electron is small, only the electrons generated within about 10[nm] under the surface come out of the surface [5, 6]. This fact means that, as shown in Fig. 3, the larger secant angle of the surface makes more secondary electrons emerge out. As the result, the total energy of the secondary electrons coming out of the surface having secant angle θ_t to the incident electron beam will be proportional to $1/\cos\theta_t$ $(= \sec\theta_t)$. If all of the electrons emerging out of the surface are captured by the detector, the brightness I of the pixel in SEM image corresponding to this surface point will be

$$I \propto \frac{1}{\cos\theta_t} \tag{1}$$

This representation is called the "secant-law" model.

Some other models were proposed based on experimental insights [1, 3, 4], such as

$$I \propto \frac{1}{\cos(k\theta_t)}\,, \tag{2}$$

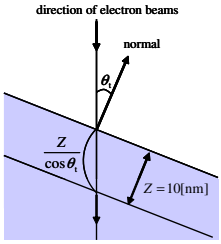

Figure 3: Relation between the total amount of the secondary electrons and surface secant angle.

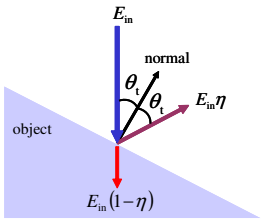

Figure 4: Incident electron beam and the reflection.

$$I \propto (1-s) + \frac{s}{\cos\theta_t} , \quad (3)$$

$$I \propto e^{\alpha(1-\cos\theta_t)} , \quad (4)$$

where k, s, and α are model's parameters.

Those models assume that the image brightness is same if the secant angle θ_t is same. However, in actual SEM images, the 1-to-1 correspondence between the brightness and the secant angle does not always hold.

3 Proposition of physics-based new model

3.1 Details of the imaging process

The SEM imaging process can be considered in detail as a sequence of next physical phenomena.

The main differences of the new model from the simple secant-law process are that all of the secondary electrons are not captured by the detector but occluded by other object surfaces and that the reflections of electrons are taken into account.

1) The incidence of the electron beam onto object surface In the SEM, high energy electron beams accelerated with 3–30[kV] electric field is projected. As shown in Fig. 4, the reflecting energy on the object surface and the energy which contributes to generate the secondary electron for the incident energy E_{in} are given as

$$E_1 = E_{in}\eta \quad \text{and} \quad E_2 = E_{in}(1-\eta) , \quad (5)$$

respectively. η is the reflection ratio of the object surface and given as

$$\eta(Z,\theta_t) = (1+\cos\theta_t)^{-\frac{9}{\sqrt{Z}}} \quad (6)$$

experimentally [6], where Z is the atomic number of the object.

2) Generation of the secondary electrons From (5) and secant-law, total amount energy of the emerging secondary electrons is given as

$$E_3 = C_1 \frac{E_{in}(1-\eta)}{\cos\theta t} \quad (7)$$

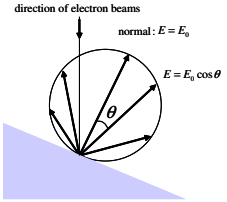

Figure 5: The directional distribution of the secondary electron flowing out of the surface.

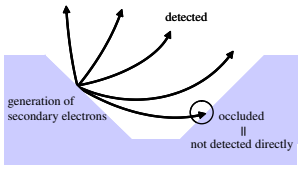

Figure 6: Occluded and detected secondary electrons.

where C_1 is a constant. If all of the emerging secondary electrons will be captured by the detector, then the brightness of the SEM image at this point is proportional to this energy.

3) Detection of the secondary electrons The emerging secondary electrons from the object surface are know to have a distribution with respect to their direction θ, which is expressed as (Fig. 5) [6],

$$\delta E = E_0 \cos\theta \delta\Omega \quad (8)$$

where E_0 is the energy released in the vertical direction of the surface and Ω is a unit steradian. From (7), the total energy of the secondary electrons emerging out into a steradian S_{se} is given as

$$E = \frac{C_1 E_{in}(1-\eta(Z,\theta_t))}{\pi\cos\theta_t} \iint_{S_{se}} \cos\theta\sin\theta \, d\theta \, d\phi \quad (9)$$

Then, the brightness of the SEM image produced by these secondary electrons is given as $I = C_2 E$.

In the conventional SEM analysis, all of the secondary electrons are believed to be detected. But, there must be possibility of the occlusion which blocks the secondary electron to reach the detector. The trajectories of the secondary electron flow draw curves under the electric field as shown in Fig. 6, and a part of the electrons can not reach the detector.

4) Reflection of the electrons on the object surface The reflecting electron beam still has as large energy E_1 as the beam originally had, so that the reflecting beam runs straight. Then, as shown in Fig. 7, it causes secondary electrons at the other surface point.

The secondary electrons generated by the reflecting electrons also suffer the occlusions if their trajectories are blocked by other object surfaces as shown in Fig. 6, and remaining electrons are detected. The energy of the reflecting electrons have directional distribution as shown in Fig. 8, where it has maximum energy in the direction of reflection angle same as the incident angle.

The secondary electrons emitted and blocked by an occluding object shown in Fig. 6 have much less energy, at most less than 50[eV], so that they can generate secondary electrons no more [6]. But, a part of them should reflect again at the occluding surface as shown in Fig. 9, and which must be taken account as the detected energy.

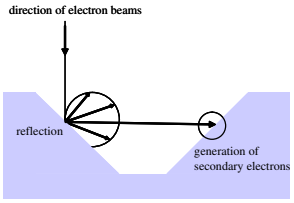

Figure 7: Reflection of the electron beam on the object surface.

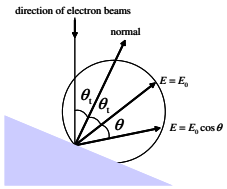

Figure 8: Distribution of the reflecting electron energy on the surface.

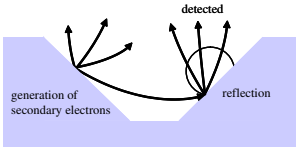

Figure 9: Reflection of the blocked electrons.

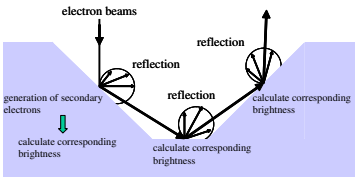

Figure 10: Schematics of the total summing up the electron energies which contribute the brightness of SEM image.

5) Total energy of the secondary electrons The number of the secondary electron which have an energy of $E_{\rm se}$[eV] is estimated by so-called the Reimer's formulation as

$$N(E_{\rm se}) \propto \frac{E_{\rm se}}{(E_{\rm se}+\phi)^4} \tag{10}$$

where ϕ[eV] is the work function of the object material. In the experiments shown later, all the secondary electrons will be assumed to have average energy derived by (10).

3.2 Total electron energy detected and the brightness of a pixel

As is schematically sketched in Fig. 10 and following the process above, the emitting and the reflecting secondary electron energies are calculated, first, in every angles to the surface, then total energy is integrated and converted into the brightness of the point at which the electron beam incidence.

For the reflection electron beam, we need to determine the reflecting angle area where the electron will be captured by the detector. Then, we calculate the brightness produced by the electrons emitted to the direction within this area. Finally, summing up the total energy of above components listed up above, we have brightness of a pixel of the SEM image.

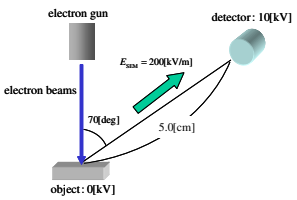

Figure 11: Dimensions of instrumentation in SEM.

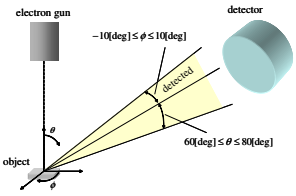

Figure 12: Spatial angle where the electrons were captured by the detector.

4 Experiments

4.1 Instrumentation set-up

We made nickel ($Z = 28$) test pieces having known dimensions and obtained their SEM images. Then we compared the actual image data and those calculated from the proposed model. We used a SEM device JEOL JSM-6460LV in the experiments. The dimensions of the instrumentation were shown in Fig. 11.

The detector was considered to have circular shape with a diameter 2[cm], so that, as shown in Fig. 12, the electrons which emitted between the spatial angles $60[\deg] \le \theta \le 80[\deg]$ and $-10[\deg] \le \phi \le 10[\deg]$ and which were not blocked were captured by the detector.

The work function of nickel is 4.6[eV] [7], then the average energy of the emitted secondary electrons is 4.5[eV] from the Reimer's (10).

4.2 Experimental results

3D shape of one of the test pieces is shown in Fig. 13(a) with its SEM image viewed from top. Figure (b) is the brightness along with the cross section line. The detector was placed at right hand side of the object.

Here after, I_{i-j} denotes captured energy of the secondary electrons generated by a beam after $i-1$ times reflection and, afterward, j times reflecting on the occluding surfaces.

We consider the components of I_{1-0}, I_{1-1}, I_{1-2}, I_{2-0}, I_{2-1}, I_{2-2}, I_{3-0}, I_{3-1}, I_{4-0}, and I_{4-1}. The captured energy of injection electron beam $E_{\rm in}$ after i times reflections is also denoted as $E_{{\rm ref}-i}$, and we also consider $E_{\rm ref-1}$, $E_{\rm ref-2}$, and $E_{\rm ref-3}$. Then, we denote the summations of $I_{1-0},\ldots,I_{4-1}$ with $I_{\rm sum}$, and $E_{\rm ref-1},\ldots,E_{\rm ref-3}$ with $E_{\rm ref-sum}$, respectively. The brightness will be $I_{\rm sum} + CE_{\rm ref-sum}$, where C is a constant.

The brightness at the top of the hill of the test piece shown in Fig. 13(a) is considered to be generated directly by the incident beam, and the coefficient C_2 is determined referring the SEM image. Then brightness components I_{1-0}, I_{1-1}, and I_{2-0} described above have profiles shown in from Fig. 14 to Fig. 16, respectively. In Fig. 17, $I_{\rm sum}$ with its actual SEM image brightness $I_{\rm real}$ is shown.

We also show $E_{\rm ref-sum}$ in Fig. 18 and $I_{\rm sum} + CE_{\rm ref-sum}$ with $C = 13.0$ in Fig. 19 with also $I_{\rm real}$. The averaged deference between $I_{\rm real}$ and $I_{\rm sum} + CE_{\rm ref-sum}$ at every point on the object surface was 11.30.

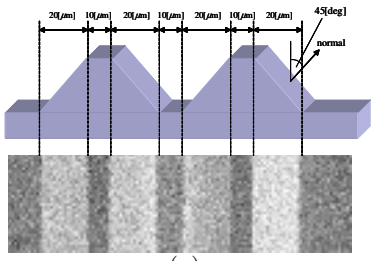

(a)

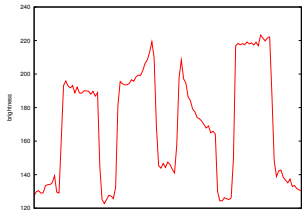

(b)

Figure 13: (a) 3D shape of a test piece and its SEM image. (b) Profile of the brightness along with a horizontal cross section line of (a).

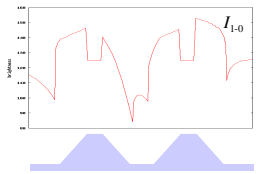

Figure 14: I_{1-0}.

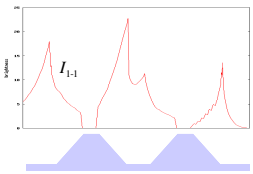

Figure 15: I_{1-1}.

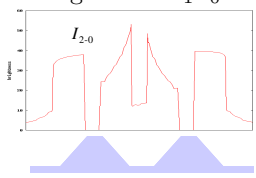

Figure 16: I_{2-0}.

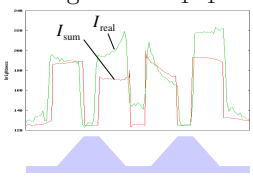

Figure 17: I_{sum} and I_{real}.

To compare $I_{\text{sum}} + CE_{\text{ref}-\text{sum}}$ with every component models, the actual brightness I_{real} is overlaid in Fig. 20 with $I_{\text{sum}} + CE_{\text{ref}-\text{sum}}$, I_{1-0}, I_{1-1}, I_{2-0}, I_{2-1}, I_{3-0}, and $CE_{\text{ref}-\text{sum}}$. I_{1-2}, I_{2-2}, I_{3-1}, I_{4-0}, are I_{4-1} are small and not shown. In the figure, increase of I_{real} at the part encircled show the same tendencies of I_{2-0}, I_{3-0} and so on. This means the proposed model represents main characteristics of the SEM image.

The difference will be decreased and the model will become more accurate if we consider that more electrons than assumed were reflected on the surface.

In the experiment, the final conversion of the electron energy to the brightness is determined with a constant C, whose exact value is left unknown. This value must be examined accounting the physical detail process of the scintillation mechanism.

By other test pieces having similar shape, we had almost similar characteristics of the SEM images.

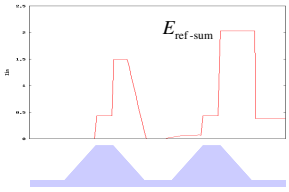

Figure 18: $E_{\text{ref}-\text{sum}}$.

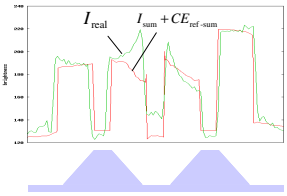

Figure 19: $I_{\text{sum}} + CI_{\text{ref}-\text{sum}}$ and I_{real}, where $C = 13.0$.

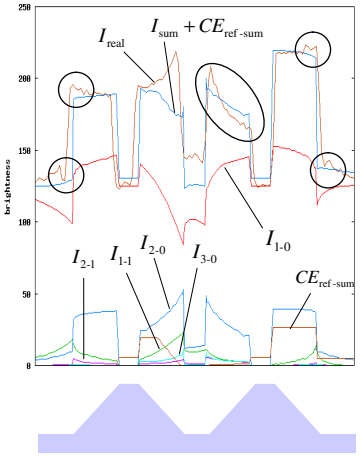

Figure 20: I_{real}, $I_{\text{sum}} + CE_{\text{ref}-\text{sum}}$, I_{1-0}, I_{1-1}, I_{2-0}, I_{2-1}, I_{3-0}, $CE_{\text{ref}-\text{sum}}$.

5 Conclusions

In this paper, we proposed a SEM imaging model by considering detail physical processes mainly reflection of the incident beam, blocking of the secondary electrons be object surfaces and the spatial configuration of the detector.

The experiments showed that the conventional models were too simple and could not describe the characteristics of the brightness distribution of the EM image, and the proposed model represents them more exactly. Further consideration of the physical process in the detector is needed.

References

[1] Katsushi Ikeuchi and Berthold K. P. Horn, Numerical Shape from Shading and Occluding Boundaries, Artificial Intelligence, vol. 17, pp. 141-184, 1981.

[2] Berthold K. P. Horn, Robot Vision, MIT Press, 1989.

[3] Pascal Daniel and Jean-Denis Durou, From Deterministic to Stochastic Methods for Shape From Shading, In Proc. of the 4^{th} Asian Conference on Computer Vision, pp.187-192, 2000.

[4] Ruo Zhang, Ping-Sing Tsai, James Edwin Cryer and Mubarak Shah, Shape from Shading: A Survey, IEEE Transactions on Pattern Analysis and Machine Intelligence, vol. 21, No. 8, pp. 690-705, August 1999.

[5] Fundaments and Aplication of Scanning Electron Microscopes (in Japanese), Kyoritsu Pub., 1983.

[6] Handbook of Scanning Electron Microscopes (in Japanese), Kyoritsu Pub., 2000.

[7] Metal Data Book (in Japanese), Maruzen Pub., 1993.